



# Measurements of Global Distributions of Polar Mesospheric Clouds during 2005-2012 by MIPAS/Envisat

Maya García-Comas<sup>1</sup>, Manuel López-Puertas<sup>1</sup>, Bernd Funke<sup>1</sup>, Á. Aythami Jurado-Navarro<sup>1</sup>, Angela Gardini<sup>1</sup>, Gabriele P. Stiller<sup>2</sup>, Thomas v. Clarmann<sup>2</sup>, and Michael Höpfner<sup>2</sup>

<sup>1</sup>Instituto de Astrofísica de Andalucía, CSIC, Granada, Spain

<sup>2</sup>Karlsruhe Institute of Technology, Institute for Meteorology and Climate Research, Karlsruhe, Germany

Correspondence to: M. López-Puertas (puertas@iaa.es)

**Abstract.** We have analysed the MIPAS IR measurements of PMCs for the summer seasons in the Northern and Southern Hemispheres from 2005 to 2012. Measurements of PMCs using this technique are very useful because they are sensitive to the total ice volume independent of particle size. For the first time, MIPAS has provided coverage of the PMCs total ice volume from mid-latitudes to the poles. MIPAS measurements indicate the existence of a continuous layer of mesospheric ice, extending from about  $\sim 81$  km up to about 88-89 km on average and from the poles to about  $50\text{--}60^\circ$  in each hemisphere, increasing in concentration with proximity to the poles. We have found that the ice concentration is larger in the Northern Hemisphere than in the Southern Hemisphere. The ratio between the ice water content (IWC) in both hemispheres is also latitude-dependent, varying from a NH/SH ratio of 1.4 close to the poles to a factor of 2.1 around  $60^\circ$ . This also implies that PMCs extend to lower latitudes in the NH. A very clear feature of the MIPAS observations is that PMCs tend to be at higher altitudes with increasing distance from the polar region (in both hemispheres), particularly equator-wards of  $70^\circ$ , and that they are about 1 km higher in the SH than in the NH. The difference between the mean altitude of the PMC layer and the mesopause altitude increases towards the poles and is larger in the NH than in the SH. The PMC layers are denser and wider when the frost point temperature occurs at lower altitudes. The layered water vapour structure caused by sequestration and by sublimation of PMCs is more pronounced at latitudes northernmost of 70 degrees. Finally, MIPAS observations have also shown a clear impact of the migrating diurnal tide on the diurnal variation of the PMCs ice concentration.

## 1 Introduction

Polar mesospheric clouds (PMCs), usually called noctilucent clouds (NLCs) when observed from the ground, occur at the coldest regions of the atmosphere near the summer high latitude mesopause. PMCs normally form a layer extending vertically for several kilometres, peaking near 83 km, located at latitudes poleward of  $50^\circ$ . In this region the temperature frequently drops below the frost point which, for mesospheric pressures and humidities, is as low as 150 K. They mainly consist of water ice particles with radii ranging from a few nm to about 100 nm (Rusch et al., 1991; Gumbel and Witt, 1998; Hervig et al., 2001; von Savigny et al., 2005).



NLCs are only the optically visible (and lower) part of the layer of icy particles covering the entire polar mesopause region (Berger and Zahn, 2002; Rapp and Thomas, 2006). However, the whole layer modifies the ambient plasma of the D-region and gives rise to intense radar echoes, the so-called PMSE (Polar Mesospheric Summer Echoes) (Rapp and Lübken, 2004). It is now generally accepted that the larger particles are located near the bottom of the layer, while the smaller ones are more likely to be near the top of the layer (Berger and Zahn, 2002; von Savigny et al., 2005; Baumgarten and Fiedler, 2008).

PMCs have been intensively studied using ground, rocket, and space observations (SNOE, SBUV, ODIN, SCIAMACHY, GOMOS, AIM) (Baumgarten and Fiedler, 2008; Fiedler et al., 2009; Gumbel and Witt, 1998; Bailey et al., 2005; DeLand et al., 2003; Petelina et al., 2006; von Savigny et al., 2005, 2007; von Savigny and Burrows, 2007; Pérot et al., 2010; Russell III et al., 2009); as well as sophisticated models (Berger and Zahn, 2002; Berger and von Zahn, 2007). A good review on our knowledge about PMCs up until 2006 was compiled by Rapp and Thomas (2006). A more recent review, including a comparison with mesospheric clouds on Mars, was conducted by Määttä et al. (2013).

PMCs are being discussed as potential early indicators of global climate change (Thomas et al., 1989; von Zahn, 2003) because they are very sensitive to temperature and water vapour concentration. Since enhanced CO<sub>2</sub> amounts (see, e.g., Yue et al., 2015) would lead to an eventual cooler upper mesosphere/lower thermosphere, and higher CH<sub>4</sub> amounts may lead to enhanced H<sub>2</sub>O near the mesopause (Roble and Dickinson, 1989; Nedoluha et al., 2009; Garcia et al., 2015), they could both lead to an increase of PMC occurrence, which might be interpreted as an effect of climate change in the upper atmosphere. There is not, however, a consensus in the scientific community about this aspect (von Zahn, 2003; Thomas, 2003). The recent study of SBUV (Solar Backscatter Ultraviolet) data from 1979 through 2013 by DeLand and Thomas (2015) has shown, in addition to the clear solar cycle signal, a good correlation with stratospheric ozone variations. Also, they have found that PMC ice water content in bright clouds increased rapidly from 1979 through the late 1990s and has been approximately constant from the late 1990s through 2013.

Hervig and Stevens (2014) calculated SBUV ice water content (IWC) values using a different method to DeLand and Thomas (2015) and compared their results with SOFIE data. They found good agreement in average IWC if an appropriate threshold was applied to the SOFIE data set, and consistent day-to-day and year-to-year variations between both data sets.

Russell et al. (2014) looked at trends in the northern mid-latitude noctilucent cloud occurrences using satellite data and model simulations and found a significant increase in the PMC occurrences at mid-latitudes from 2002 to 2011. This result differs somewhat from the insignificant trend found by DeLand and Thomas (2015) for a similar period but at higher latitudes.

Berger and Lübken (2015) analysed trends in mesospheric ice layers in the high latitude Northern Hemisphere for the 1961–2013 period with model simulations. They reported a generally good agreement between long-term PMC variations from the MIMAS model and the SBUV satellite observations. They found that the modelled trends in ice water content are latitudinally dependent with no clear trend at mid-latitudes (50°–60°N) but with a clear positive trend at high latitudes (74°–82°N) and also in extreme PMC events.

Thomas et al. (2015) have studied the solar-induced 27-day variations in polar mesospheric clouds using 15 seasons of data taken by the SOFIE instrument and suggested that the changes in the PMCs are due to 27-day variations of vertical winds.



As described above, a large fraction of the observations taken so far were performed by measuring the scattered light, in the visible or UV, of the solar radiation (in the case of instruments from space) or of the lidar light (in case of ground instruments). This technique usually observes the ice particles with radii larger than about 20 nm but lacks sensitivity for smaller particles (see, e.g., Rapp and Thomas, 2006). A different technique, however, has been used recently by the AIM/SOFIE (Aeronomy of  
5 Ice in the Mesosphere/Solar Occultation for Ice Experiment) instrument. These measurements have provided key characteristics of PMC's such as their frequency, mass density, particle shape, and size distribution, as well as their seasonal evolution and altitude dependence (see, e.g. Hervig et al., 2009a, b, 2011, 2013). Furthermore these satellite data have supplied critical information about the relationship of the ice density distribution with mesopause temperature and water vapour concentration (see, e.g. Hervig et al., 2009c; Russell et al., 2010; Hervig et al., 2015).

10 While PMCs emit thermal radiation, their infrared emissions are very difficult to observe due to the low ice particle volume density and the very cold polar summer mesopause temperatures. In fact, only three IR emission observations have been reported to date: that taken by CRISTA (Grossmann et al., 2006), by the SPIRIT (O'Neil et al., 2008) and those taken by MIPAS (López-Puertas et al., 2009). This technique has the advantages of being able to measure PMCs in dark conditions –thus providing a better spatial coverage–, and of being sensitive to the total ice volume density, regardless of particle size, and  
15 hence including the very small particles.

In this previous paper (López-Puertas et al., 2009) we reported the detection of infrared emissions from PMCs taken by the Michelson Interferometer for Passive Atmospheric Sounding (MIPAS) instrument on board ENVISAT (Environmental Satellite), and provided further evidence of the water ice nature of the PMC particles. We also described the retrieval of the ice particle volume density and reported the analysis of the retrieved densities for 19-21 July 2005. In this paper we present the  
20 global distributions (altitude, latitude and longitude) of the ice volume density measured by MIPAS for several days in each of the Northern (NH) and Southern Hemisphere (SH) seasons from 2005 until early 2012. We also analyse several aspects of the PMCs such as: (i) the mean altitude of the layer, the ice water content and their hemispheric dependence; (ii) the correlation of the ice volume density with the frost point temperature and with the water vapour concentration; and (iii) the diurnal variation of the ice volume density. MIPAS, as well as SOFIE, has the advantage of measuring the whole content of ice particles (all  
25 sizes) in the mesosphere. Hence, a comparison with SOFIE observations is also shown.

## 2 MIPAS Measurements and Ice Density Retrieval

MIPAS is a high-resolution limb sounder on board the ENVISAT satellite, launched on March 1, 2002. It took measurements until 8 April 2012, when the Envisat satellite failed. MIPAS measurements covered a wide spectral range with a high spectral resolution, operating at  $0.025\text{ cm}^{-1}$  from 2002-2004 and  $0.0625\text{ cm}^{-1}$  from 2005 until the end of the mission. It also  
30 operated with a high sensitivity, allowing measurement of most of the atmospheric emissions in the mid-infrared over a large altitude range (Fischer et al., 2008). MIPAS operated with a global latitude coverage (pole-to-pole) and performed measurements irrespective of day- or night-time. The instrument spent most of the time observing in the 6-68 km altitude range (the



**Table 1.** Days of MIPAS observations of PMCs in the different modes.

Mode	Days									
NLC	20050719	20050720	20050721	20070704	20070705	20070714	20070715	20080705	20080706	
	20080707	20090105	20090106	20090107	20090705	20090706	20090707	20100104	20100105	
	20100106	20100703	20100704	20100705	20110109	20110110	20110111	20110708	20110709	
	20110710	20120104	20120105	20120106						
MA	20050110	20050111	20050112	20050113	20051229	20051230	20060621	20060622	20061219	
	20061220	20061221	20070622	20070725	20070804	20071219	20071229	20080108	20080116	
	20080126	20080205	20080616	20080625	20080715	20080725	20080804	20081222	20090101	
	20090111	20090205	20090615	20090625	20090715	20090725	20090801	20090811	20091215	
	20091225	20100114	20100122	20100613	20100623	20100713	20100723	20100802	20100812	
	20110119	20110618	20110628	20110719	20110801	20110807	20111225	20120114		
UA	20050121	20050122	20050722	20051231	20060623	20061222	20070620	20070621	20071220	
	20071230	20080109	20080117	20080127	20080206	20080622	20080716	20080726	20080805	
	20081223	20090102	20090112	20090119	20090120	20090206	20090616	20090626	20090716	
	20090726	20090802	20090812	20091220	20091230	20100109	20100117	20100618	20100628	
	20100718	20100728	20100807	20100817	20101225	20110104	20110114	20110124	20110130	
	20110131	20110201	20110623	20110703	20110714	20110727	20110804	20110812	20111220	
	20111230	20120109	20120124							

nominal mode) but it also regularly observed at higher altitudes in its middle atmosphere (MA), noctilucent (NLC), and upper atmosphere (UA) modes (De Laurentis, 2005; Oelhaf, 2008).

In the MA mode, the spectra are available at limb tangent heights from about 20 km up to 102 km with a vertical sampling of 3 km. The UA mode ranges from about 42 km to 172 km, and has a vertical sampling of 3 km up to 102 km, and 5 km above this altitude. The NLC mode is a variant of the middle atmosphere mode specifically tailored for measuring the PMCs during the summers (De Laurentis, 2005; Oelhaf, 2008). In this mode the spectra cover tangent heights from 39 km up to 78 km at 3-km steps; then from 78 km up to 87 km at 1.5 km steps, and from 87 km up to 102 km again in 3-km steps. MIPAS horizontal field of view (FOV) is approximately 30 km. The days of PMC measurements in the different observation modes are listed in Table 1, and a summary of the distribution of these days along the different seasons is shown in Table 2.

The method used for the inversion of PMC ice volume density from the MIPAS spectra has been described in López-Puertas et al. (2009). A brief excerpt is included here. The spectra analysed in this work were all taken with the optimized spectral resolution of  $0.0625 \text{ cm}^{-1}$ . The ice volume density was retrieved from the radiance profiles obtained by integrating the spectra from  $730 \text{ to } 950 \text{ cm}^{-1}$ . The profiles were corrected for an offset variable in altitude, latitude and time.



**Table 2.** Distribution of MIPAS days of observation of PMCs per season\* .

Year	NLC		MA		UA		Total	
	NH	SH	NH	SH	NH	SH	NH	SH
2005	3	-	-	4	1	2	4	6
2006	-	-	2	2	1	1	3	3
2007	4	-	3	3	2	1	9	4
2008	3	-	5	6	4	6	12	12
2009	3	3	6	4	6	6	15	13
2010	3	3	6	4	6	4	15	11
2011	3	3	5	1	6	7	14	11
2012	-	3	-	2	-	4	-	9
Total	19	12	27	26	26	31	72	69

\* For the NH season the days correspond to June-August of the listed year. For SH season the days correspond to December of the preceding year and January-February of the listed year.

The noise equivalent spectral radiance in this spectral region is about  $20 \text{ nW}/(\text{cm}^2 \text{ sr cm}^{-1})$ , and the corresponding noise in the integrated radiances of a single scan is  $\sim 60 \text{ nW}/(\text{cm}^2 \text{ sr})$ .

The ice volume density was retrieved from the spectrally-integrated radiance profiles using a linearly constrained least squares fitting, where the Jacobians were calculated using the KOPRA radiative transfer algorithm (Stiller et al., 2002). The inversion was constrained by a Tikhonov-type scheme (Tikhonov, 1963) using a squared first-order differences matrix to obtain a reasonably smoothed vertical profile of volume densities. The ice refractive indices were taken from Toon et al. (1994).

In this analysis we have included the following improvements and updates with respect to López-Puertas et al. (2009): (i) The more recent version 5 (5.02/5.06) of MIPAS L1b spectra has been used; (ii) an updated version of the temperature is used for the retrieval of ice density (see below); (iii) the altitude registration of the L1b spectra has been improved by using the information from the retrieved temperature and LOS (line of sight) instead of the engineering information included in the L1b files (von Clarmann et al., 2003; García-Comas et al., 2012); (iv) the offset correction of the integrated radiance profiles was improved by taking into account its altitude and latitudinal variations; (v) the ice density profiles were retrieved only for the scans with converged pressure-temperature profiles (no latitude/longitude interpolation was done); and (vi) due to a mistake in the calculation of the volume of the particles distribution, the volume densities presented here are nearly double those previously reported in López-Puertas et al. (2009).

The temperature and LOS required to retrieve the ice density have been inverted from the  $\text{CO}_2$  emission near  $15 \mu\text{m}$ , recorded in the same MIPAS band A as the PMC emission. Non-local thermodynamic equilibrium (non-LTE) emission was taken into account. The detailed description of the method and the characterization of the inverted temperature profiles are described in



García-Comas et al. (2012). The upgrades in the retrieval of the temperature used here (version vM21) and a validation of the results are reported by García-Comas et al. (2014). Briefly, these authors include an updated version of the calibrated L1b spectra in the 15  $\mu\text{m}$  region (versions 5.02/5.06); the HITRAN 2008 database for CO<sub>2</sub> spectroscopic data; the use of a different climatology of atomic oxygen and carbon dioxide concentrations; the improvement of several aspects of the retrieval set-up  
5 (temperature gradient along the line of sight, offset regularization, and the spectral apodization); and some minor corrections to the CO<sub>2</sub> non-LTE modelling as detailed by Funke et al. (2012). This version of MIPAS temperatures correct the main systematic errors of the previous version and have, in general, a remarkable agreement with the measurements taken by ACE-FTS, MLS, OSIRIS, SABER, SOFIE and the Rayleigh lidars at Mauna Loa and Table Mountain. In the region of interest here, however, there are still significant differences, with MIPAS polar summer mesopause temperatures differing by 5-10 K from  
10 the other instruments, being warmer than SABER, MLS and OSIRIS and colder than ACE-FTS and SOFIE.

Since MIPAS measures PMCs in emission, knowledge of the temperature of the ice particles is crucial. There is still disagreement about the temperature of the particles, particularly if they are warmer or colder than the ambient atmosphere. Using SOFIE measurements, Hervig and Gordley (2010) have found that the ice particles are about 5-20 K cooler than the ambient temperature. They suggested, however, that the V1.022 SOFIE CO<sub>2</sub> temperatures they used might have a warm bias of  
15 5-10 K near the polar summer mesopause. Petelina and Zasetsky (2009), using infrared solar occultation measurements from the Atmospheric Chemistry Experiment (ACE) instrument, also found that the ice particles are cooler than the ambient temperature. They argue that this might be caused by inhomogeneities in the temperature along the instrument field of view, with the ice particles sensing only the cold(er) parcels, where they are present, while the gas temperature is representative of the whole (warmer) air mass along the FOV. Physical considerations, however, would suggest that the particles are warmer than  
20 the surrounding gas because they will be heated up by absorption of radiation (Rapp and Thomas, 2006; Espy and Jutt, 2002). For example, for a particle distribution with a mean radius between 30 and 50 nm and an accommodation coefficient of 0.5, Rapp and Thomas (2006) found that the ice particles are warmer than the ambient gas in about 1 K at 80 km and 2 K at 90 km. Analogously, the model calculation of Espy and Jutt (2002), when applied to a normal distribution of ice particle size with a mean radius varying from 40 nm at 80 km to 15 nm at 90 km, gives a temperature increase of 0.7 K at 80 km and 2.7 K at  
25 90 km. As suggested by these models, we applied a temperature correction of the emitting particles that varies linearly from 1 K at 80 km to 2 K at 90 km. In principle, MIPAS measurements should also be affected by the problem pointed out by Petelina and Zasetsky (2009). However, our observations do not support that finding. If we assume that the ice particles are cooler than the retrieved gas temperature we would obtain very high (and unreasonable) concentrations of ice particles (see Sec. 3).

30 The vertical resolution of the ice density vertical profiles, in terms of the half-width of the columns of the averaging kernel matrix depends on the observational mode. For the over-sampled NLC mode, it varies from  $\sim 2.5$  km at 81–82 km to  $\sim 3$  km at 86 km, and to 3.5–4 km at 90 km. For the middle and upper atmosphere modes (MA and UA), it is coarser, with values ranging from 3.5 to 4 km. The error in the absolute pointing is about 200 m.

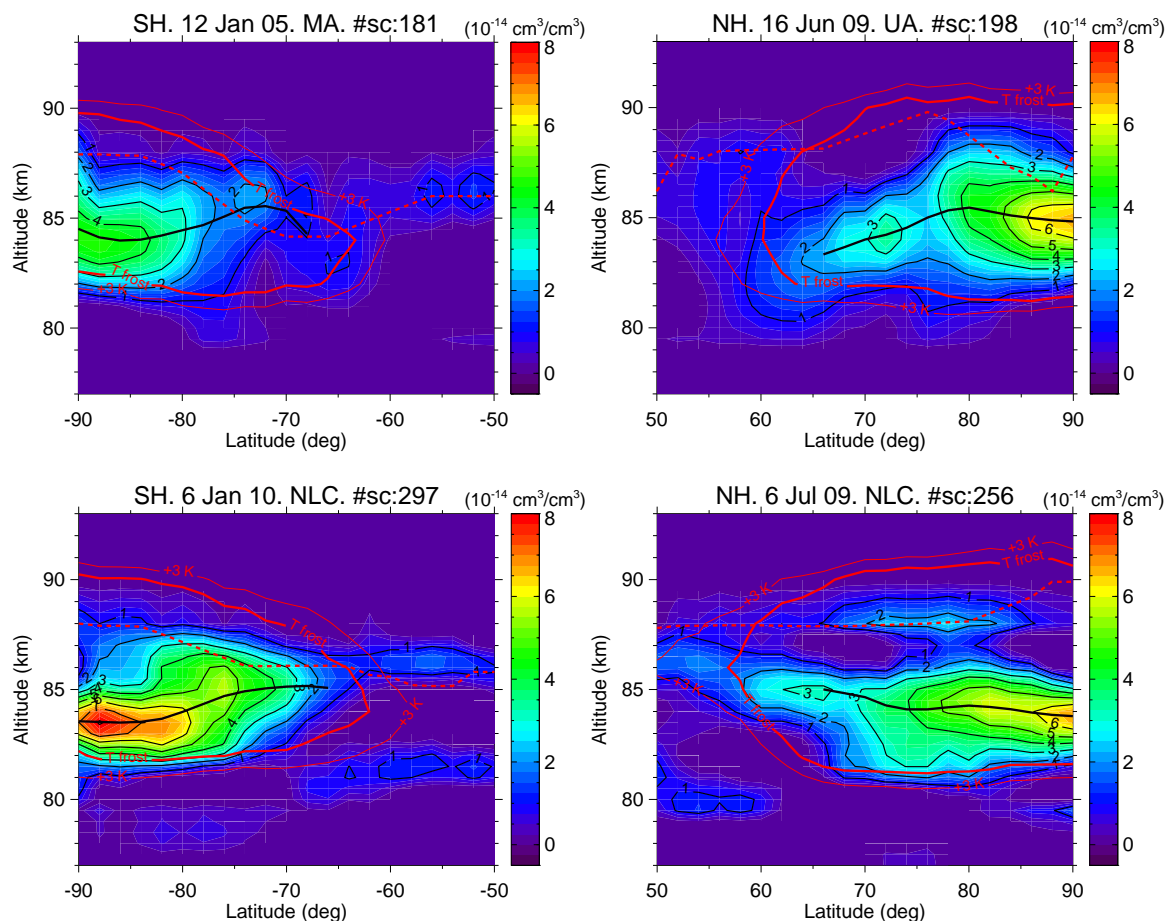


**Figure 1.** Zonal mean of ice volume density for four days, two in the Southern Hemisphere and two in the Northern Hemisphere as measured by MIPAS in different observation modes (MA, UA and NLC, see labels). The solid red lines indicate the frost point temperature (thick line) and frost point temperature plus 3 K (thinner line). The red dashed line is the mesopause as measured by MIPAS. The black solid line is an estimated mean altitude (weighted with the ice density to power of 4) of the PMC layer. The estimated noise error of the volume density plotted here is about  $0.3 \times 10^{-14} \text{ cm}^3/\text{cm}^3$ .

The averaging kernels shown in López-Puertas et al. (2009) are for the NLC mode measurements that have a sampling step (i.e. tangent altitude increment) of 1.5 km. For the MA and UA modes the averaging kernels are wider because of the coarser sampling of 3 km.

The random single profile error of the retrieved ice volume density is about 60%, including both the instrumental noise and the temperature noise error. The systematic error is about 25-30% and is mainly due to the temperature error in the summer mesopause region (García-Comas et al., 2014). More details of the retrieval of the ice volume density can be found in López-Puertas et al. (2009).

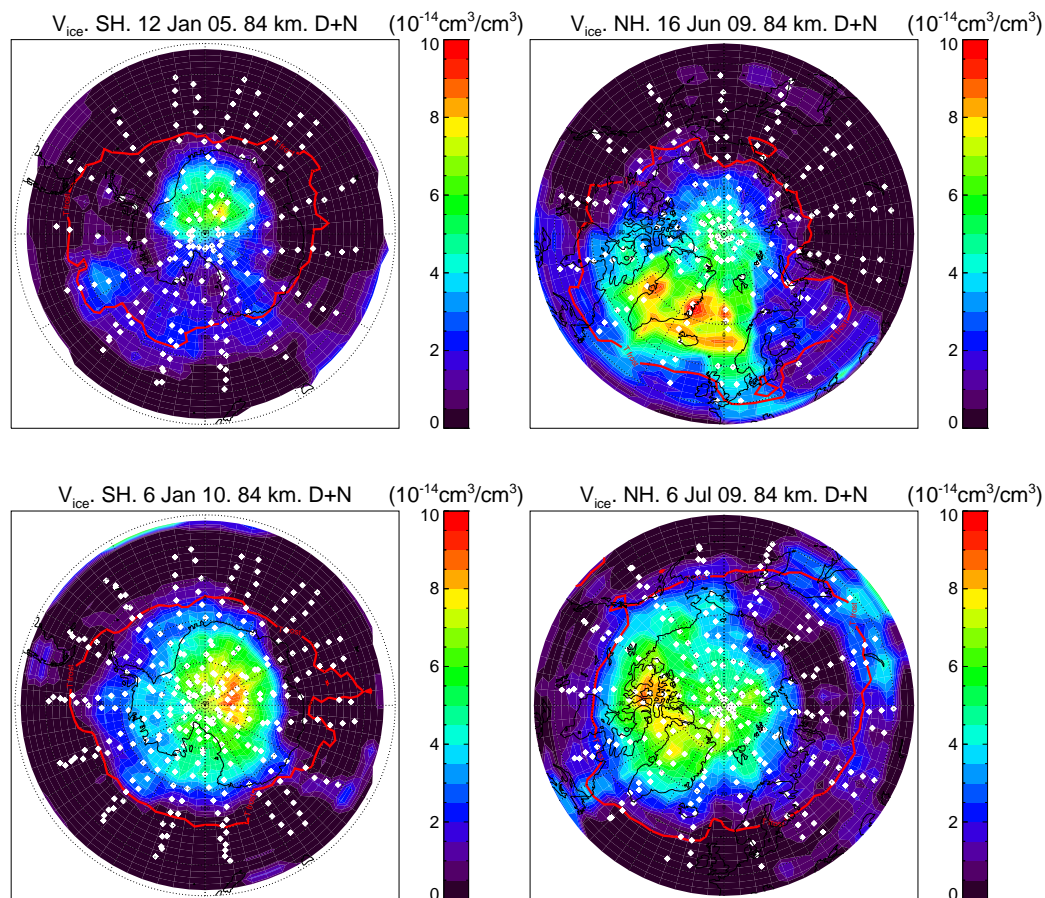


**Figure 2.** Latitude/longitude distribution maps of ice volume density at 84 km for the same days as in Fig. 1. The solid red lines indicate the frost point temperature. The diamonds represent the geolocations of the MIPAS measurements.

### 3 Ice volume density distributions

Figure 1 shows typical daily zonal means of ice volume density retrieved from MIPAS for four days in SH and NH summer seasons in different observation modes. The thick solid red line is the frost point temperature contour, and the red dash the mesopause altitude. The solid black line is an estimated altitude of the PMC layer (i.e., the altitude weighted with the 4th power of the density). Note that MIPAS measurements are sensitive to all ice particles, including those with small radius. Noise errors in these plots are about  $0.3 \times 10^{-14} \text{ cm}^3/\text{cm}^3$ . The PMCs are generally located at regions colder than the frost point temperature for almost all conditions. Note also the large variability in latitude and altitude of the ice density, particularly on 6 July 2009 (bottom right panel) where the PMCs reach latitudes as low as  $60^\circ\text{N}$ .

Anomalous low-altitude detection of weak PMCs (i.e., below  $\sim 80$  km and outside of the  $T_{frost}$  region) could be due to the limb nature of the measurements. Emission from isolated clouds located in the LOS far away from the tangent point, and



hence at higher altitudes, can be measured and thus attributed to these lower tangent heights (see, e.g., Hervig et al. (2009b), their Fig. 11). Also, the FOV can affect the lower and upper boundaries of the layer. Hervig et al. (2009b) have shown that the bottom and top altitudes as measured by SOFIE, which has a FOV of 1.5 km, can be smeared out in about 1-1.5 km. These two effects, along with the temperature error, can explain why MIPAS observes occasional ice volume concentration at the bottom of the layer at temperatures warmer than the frost point temperature, see bottom-left panel of Fig. 1 around 70°N.

The latitude/longitude distributions of ice volume density at 84 km for corresponding days are shown in Figure 2. As shown before for the zonal means, the PMC layer is almost always confined to regions with temperature below the frost point temperature. The variability of the latitude/longitude spread is also large. Although the PMCs are generally centred around the pole, they are sometimes far away (see top right panel in Fig. 2).

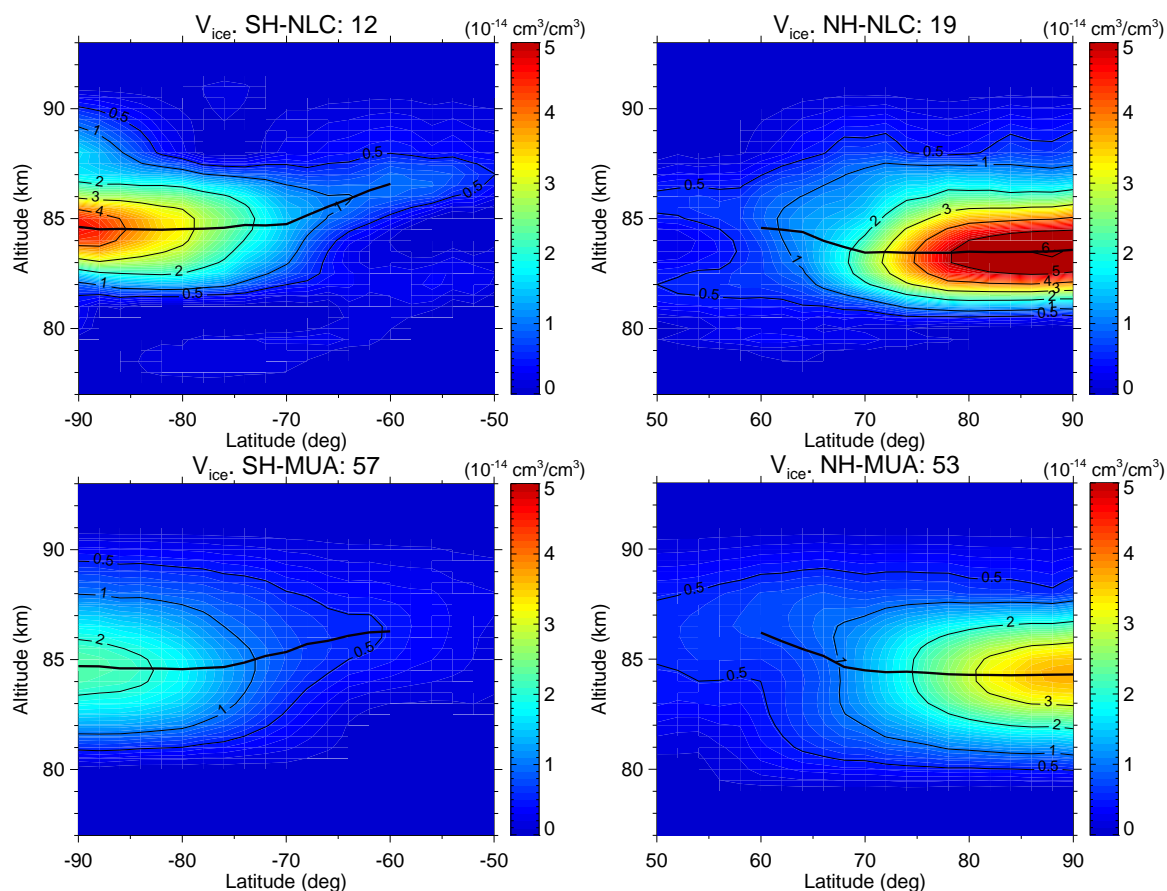


**Figure 3.** Zonal mean distributions of ice volume density for all measured days in the Southern (left panels) and Northern (right panels) hemispheres for the NLC (top panels) and for the MA+UA (MUA) (lower panels) MIPAS modes (see Table 2). The solid black line is an estimated mean altitude (weighted with the ice density to power of 4) of the PMC layer. The estimated noise error of the volume density plotted here is about  $0.08 \times 10^{-14} \text{ cm}^3/\text{cm}^3$  and  $0.04 \times 10^{-14} \text{ cm}^3/\text{cm}^3$  for the NLC and MUA measurements, respectively.

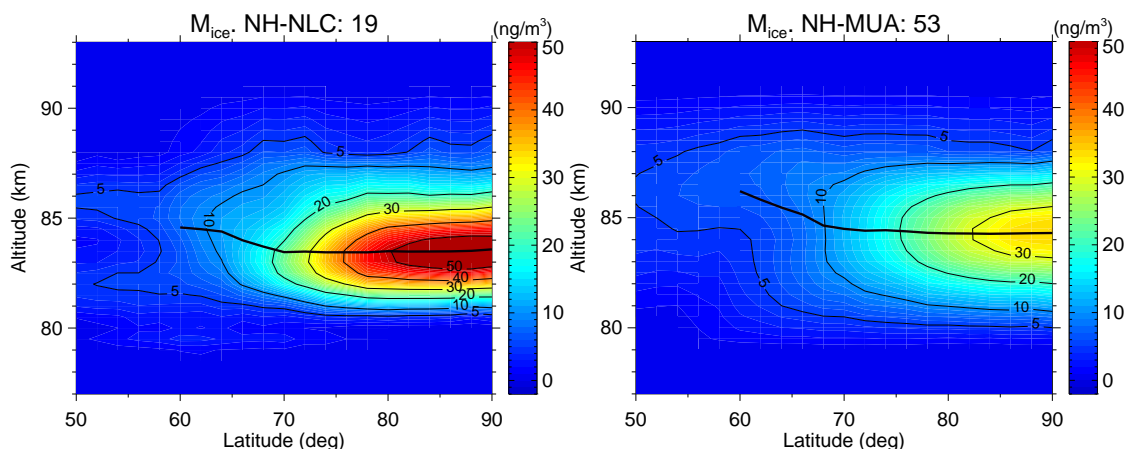


**Figure 4.** Zonal distribution of ice mass density for all measurements (see Table 2) in the Southern (left) and Northern (right) hemispheres. The solid black line is an estimated mean altitude (weighted with the ice density to the 4th power) of the PMC layer. The estimated noise error of the mass density plotted here is about  $0.8 \text{ ng/m}^3$  and  $0.4 \text{ ng/m}^3$  for the NLC and MUA measurements, respectively.

Figure 3 shows the zonal mean distributions of ice volume density averaged for all measured days in the Southern (left) and Northern (right) hemispheres for the NLC (top panels) and for the MA+UA (MUA) (lower panels) MIPAS modes (see Table 2). These distributions are analysed in detail later, but we describe the main features briefly here: 1) PMCs are confined to altitudes between around 81 km and 89 km with maximum concentrations around 84 km; 2) PMCs are confined to latitudes poleward of about  $60^\circ$ , with increasing concentration towards the poles; 3) From these figures it is evident that the ice particles occur in higher concentrations in the NH, and that the ice layer is located at slightly lower altitudes in the Northern Hemisphere. These figures also show an apparent higher concentration for the measurements taken in the NLC mode than in the MUA mode. The NLC mode has a better vertical resolution, which leads to sharper temperature profiles (see García-Comas et al., 2014) and hence to sharper ice particle profiles and larger ice particle densities. However, not all the differences between the NLC and the MUA modes can be attributed to the better vertical resolution of the former because they were taken in the summer on different days, with those of the NLC mode closer to the peak of the PMCs season.

### 3.1 Top altitude

Figure 3 shows that MIPAS observes significant abundances of ice up to about 88-89 km. A similar behaviour has been found in the SOFIE IR extinction measurements (Hervig et al., 2009b). This altitude is about 3-4 km higher than the average maximum altitude of 84.4 km measured by the lidars. Hervig et al. (2009b) have shown for SOFIE that the vertical smoothing of the limb view geometry can cause an extension of the uppermost altitude of about 2/3 of the vertical resolution, i.e., 1.5-2 km for the MIPAS NLC observation mode. This, however, cannot fully explain that difference. The detection of PMCs by SOFIE and MIPAS at altitudes higher than the lidars is most likely due to the different sensitivities of the two techniques. While the lidar signal varies with  $r^6$ , the MIPAS (in IR emission) and SOFIE (in IR extinction) signals change with the total ice volume density. As the ice particle size decreases towards higher altitudes (Baumgarten and Fiedler, 2008; Hervig et al.,



2009b; Pérot et al., 2010), MIPAS and SOFIE are then more sensitive than the lidars to higher altitude PMCs. The highest altitude of PMCs derived from MIPAS NLC mode measurements is about 89 km for the NH near 70° (Fig. 3b). This is slightly higher than that obtained by SOFIE of  $86.8 \pm 2.1$  km but agrees very well with the CARMA model prediction of  $88.5 \pm 0.5$  km (Hervig et al., 2009b, 2013). Thus, as pointed out by López-Puertas et al. (2009) and Hervig et al. (2009b), MIPAS and SOFIE results are consistent with the current understanding of temperatures and water vapour distributions at these altitudes (Lübken, 1999), and the associated ice particles at high altitudes are likely to be related to polar mesosphere summer echoes (e.g., Rapp and Lübken, 2004). This has also been evidenced more recently by the concurrent observations from the ALOMAR wind (ALWIN) radar and measurements from SOFIE (Hervig et al., 2011).

### 3.2 Bottom altitude

10 The bottom altitude of the PMC layers measured by the lidar measurements in the Northern Hemisphere (at a latitude close to 70°) was found at 82.2 km. SOFIE obtained a slightly lower altitude of 81.6 km, which is within their mutual standard deviations (Hervig et al., 2009b). For the NH and similar latitudes MIPAS in its NLC mode (see Fig. 3b) gave an altitude of ~81 km, slightly lower than SOFIE. Note, however, that we have not excluded any PMCs here, whereas in SOFIE those found below 79 km were excluded. The bottom altitude also changes rapidly with latitude from 65 to 75° (Fig. 3b); hence a few degrees in latitude might also induce a significant change in the bottom altitude. Thus, in summary, we can conclude that they are in good agreement. It is also worth noting that the bottom altitude derived from the MUA modes, which have a coarser vertical sampling (3 km), is lower by about 1 km than that derived from the NLC mode (Fig. 3d). This is very likely due to the limb sounding geometry, as discussed above. The bottom altitude in the Southern Hemisphere is found to be located at about 1 km higher than in the NH (see Figs. 3a and 3c).

### 20 3.3 Concentration

As discussed above, MIPAS and SOFIE/AIM are the only two instruments whose ice concentration data are comparable because they both measure the total ice volume density, irrespective of the ice crystal size. Although it is not the aim of this paper to carry out a detailed comparison or validation, we include some comparisons here. First, we compare the maximum (peak) values of the PMC layer, and then we compare mean profiles for several seasons.

25 SOFIE measured ice mass densities at the altitude of maximum concentration,  $z_{max}$ , for the 2007 NH season that range from 0.1 to  $80 \text{ ng m}^{-3}$ , with a mean value of  $14.2 \text{ ng m}^{-3}$  (Fig. 14a and Table 5 in Hervig et al., 2009b). These SOFIE measurements were taken at latitudes between 66°N, in the early season, to 74°N, towards the end of the season. MIPAS measurements for the 2005-2012 period at those latitudes have mean values of just above  $20 \text{ ng m}^{-3}$  for the NLC mode and of  $\sim 12 \text{ ng m}^{-3}$  (with a broader peak) for the MUA modes (see Figs. 4b and 4d, respectively), which agree well with SOFIE data for the 2007 NH season. As a result, the conclusion drawn by Hervig et al. (2009b) from SOFIE applies to the comparison of MIPAS with other measurements and models. That is, MIPAS ice mass densities are also significantly smaller than the lidar measurements taken at ALOMAR (69°N), that present an average value of  $47.4 \text{ ng m}^{-3}$ , and the lidar results reported by von Cossart et al. (1999), with ice mass ranging from 36 to  $102 \text{ ng m}^{-3}$ . MIPAS, as well as SOFIE, also measure thinner ice clouds than other

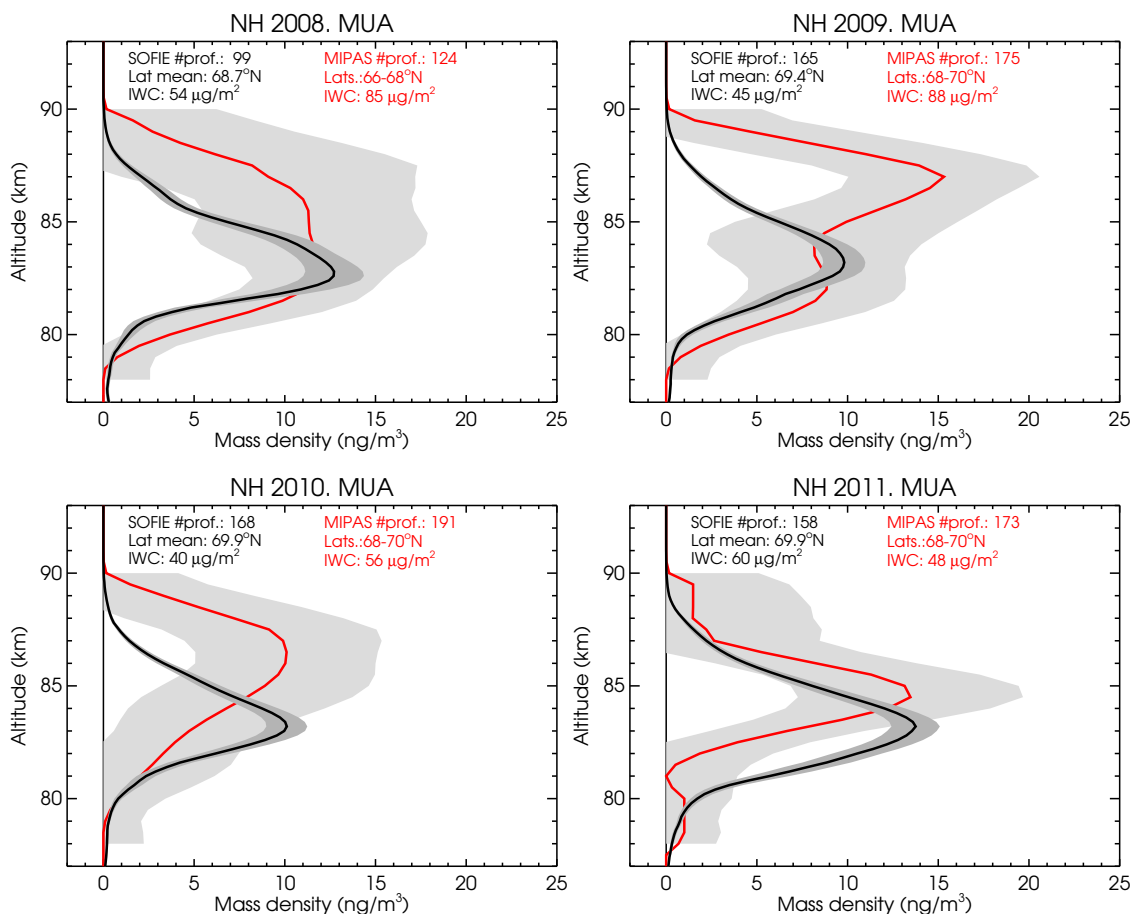


**Figure 5.** Comparison of the ice mass density of MIPAS MA and UA modes of measurements (see Table 1) with SOFIE v1.3 L2 data for the 2008 to 2011 period in the NH. The solid lines show the mean profiles, SOFIE in black and MIPAS in red. The shaded areas are the standard deviations divided by the square root of the number of profiles. The means of the integrated water column (IWC) are also shown.

IR instruments measuring the PMCs from space, e.g., HALOE (Hervig et al., 2003). Those differences can be explained, at least partially, by the larger sensitivity of MIPAS (and SOFIE) to the smaller particles (i.e., being sensitive to smaller amounts leads to lower mean concentrations). Another reason causing the differences could be, at least for the lidar observations, the averaging over the relatively larger atmospheric volumes sampled by MIPAS (and SOFIE).

5 Although a detailed comparison with the Community Aerosol and Radiation Model for Atmospheres (CARMA) (Rapp and Thomas, 2006) has not been performed, the results reported in Hervig et al. (2009b) suggest that MIPAS and CARMA are in agreement, at least for the 65-75° latitudes. A thorough comparison with the CARMA model, including higher latitude regions, is necessary but is beyond the scope of this paper.

Figure 5 shows a more detailed comparison between MIPAS and SOFIE ice mass densities,  $M_{ice}$ , for the coincident days and  
 10 latitudes in the NH season for the years with more coincident data: 2008-2011. The comparison is based on the mean profiles



for all days of measurements for each season/year for each instrument because of the large variability of the ice concentration (see, e.g. Fig. 1 in the case of MIPAS). The solid black lines represent the mean of the SOFIE measurements and the solid red line the MIPAS ice mean mass density. As discussed before, these figures also show that, in general, there is a very good agreement between the two instruments in the peak values of the layer (the 2009 NH season is an exception). However, above  
5 about 85 km, MIPAS values are nearly double those measured by SOFIE (except in 2011). This MIPAS data feature, of large ice densities at high altitudes, can also be seen in the zonal mean distributions (Fig. 4, bottom right panel): the high values above 84 km extend from the North pole to fairly low latitudes, near 70°N or even lower. The same behaviour is seen in the MIPAS data for the SH (see left panels in Fig. 3). This seems to be a clear characteristic of MIPAS measurements but absent in SOFIE. We do not have a plausible explanation for this difference. In this region the ice particles are the smallest and it could  
10 be that MIPAS is more sensitive than SOFIE to those particles. Another possible reason could be a negative bias of MIPAS temperature at those altitudes/latitudes which would result in a higher ice mass density, but such a bias present only in those localized regions seems unlikely. Note also that this zonal distribution of the ice density in MIPAS is consistent with the water vapour (gas phase) latitudinal distribution measured by MIPAS (see Fig. 10), since the depletion of water vapour near 60-70°N occurs at higher altitudes than near the North pole.

15 The integrated water column, which is written for both instruments in Fig. 5, is generally larger in the case of MIPAS, which essentially reflects the higher values in the ice mass densities of MIPAS at altitudes above ~84 km discussed above. It is noteworthy, however, that MIPAS observations are in better agreement than SOFIE with model calculations carried out by Hervig et al. (2009c) (see their Fig. 5d).

### 3.4 $Q_{ice}$

20 We also show in Fig. 6 the zonal mean of ice volume density (similar to Fig. 3) but in units of ppmv,  $Q_{ice}$ ; i.e., the partial concentration of water vapour if all the ice were to sublimate. For that conversion we used the pressure and temperature measured by MIPAS (García-Comas et al., 2014). As expected they show the same general behaviour as discussed above for the volume density. We note in general that the amount of water vapour in the form of ice ranges from 1 to 3 ppmv, although close to the North pole during the high season period (NLC) it can be as much as 6 ppmv. We think this is an important result  
25 since, to our knowledge, the water ice content has not been measured at latitudes higher than ~75°. Again these values are in good agreement with SOFIE measurements. Hervig et al. (2015) have shown time series of SOFIE  $Q_{ice}$  for the 2007-2013 period for the Northern and Southern hemispheres. The NH mid-summer values range from 2 to 3.3 ppmv, which compare well with those shown in the right panels of Figure 6 at the latitudes of SOFIE measurements, ~66°-74°N. Similarly, for the SH they show values spanning from 1.5 to 2.5 ppmv, also in good agreement with those of MIPAS shown in the left panel of  
30 Figure 6. This point is discussed further in Sec. 6.

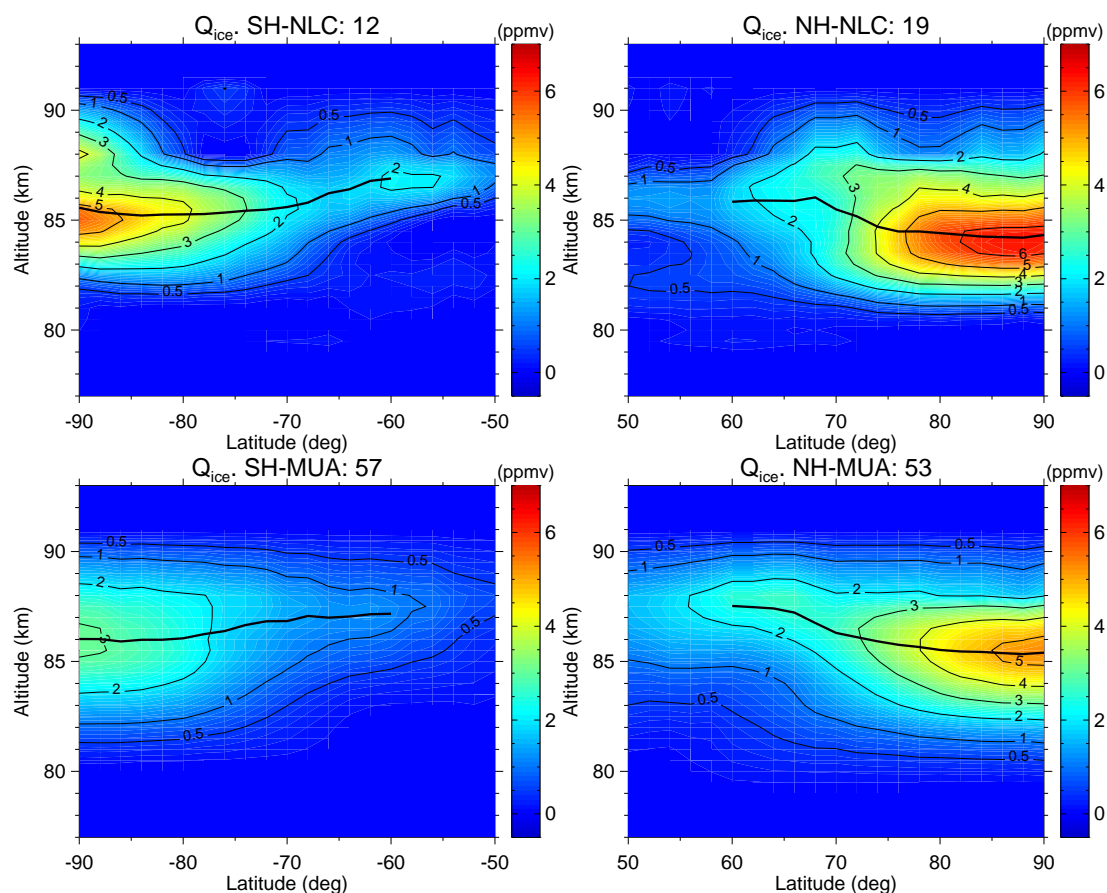


**Figure 6.** Same as Fig. 3 but in units of ppmv. The estimated noise error of the H<sub>2</sub>O ice concentration plotted here is about 0.08 ppmv and 0.04 ppmv for the NLC and MUA measurements, respectively.

#### 4 Altitude and column density of the PMCs

Figure 7 shows the mean altitude of the PMC layer for the SH (left) and the NH (right) seasons for all measurements. We observe that the mean altitude in the NH for the NLC mode is located around 83.5-84 km, while in the SH it is about 1 km higher (84.5-85 km). The fact that the mean altitude is higher (in ~1 km) for the MA+UA modes is attributed to the coarser sampling and to the broader vertical resolution in the retrieved temperature from these modes. The different temporal sampling of the NLC and MUA modes might also have an effect though. Hervig et al. (2013) have shown that PMCs are located higher at the beginning and the end of the season, and lower in the middle of the season. This coincides with our results since the NLC measurements are usually taken in the middle of the PMC season while MUA are taken earlier and later in the season. We should also note from Fig. 7 that PMCs tend to be located at lower altitudes near the poles, and at higher altitudes towards mid-latitudes (both in NH and SH but more clearly in the latter).

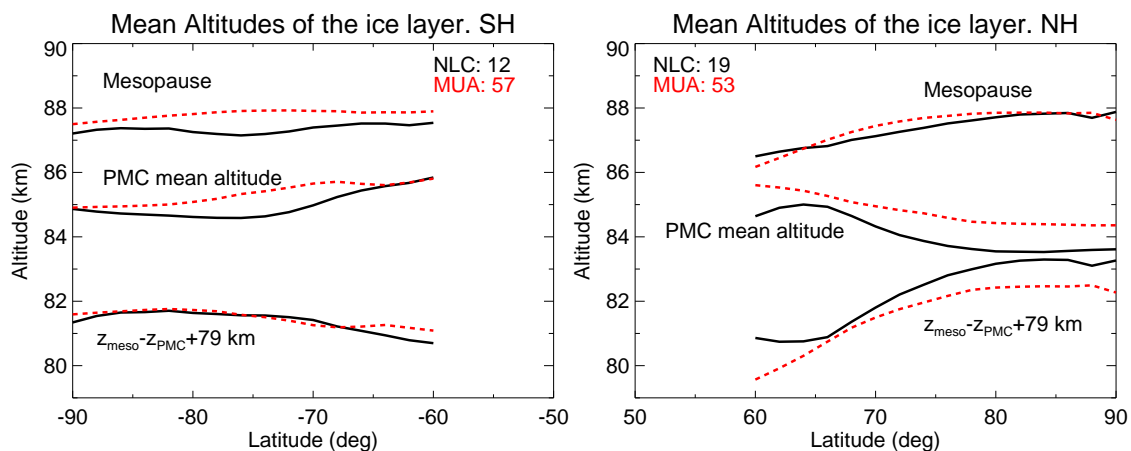


**Figure 7.** Mean altitudes of the mesopause ( $z_{\text{meso}}$ ), of the PMC layer ( $z_{\text{PMC}}$ ), and the difference  $z_{\text{meso}} - z_{\text{PMC}}$  shifted 79 km, for the SH (left) and the NH (right) seasons for all measurements. The different colors indicate the results for the NLC and MA+UA (MUA) MIPAS observation modes (see Table 2).

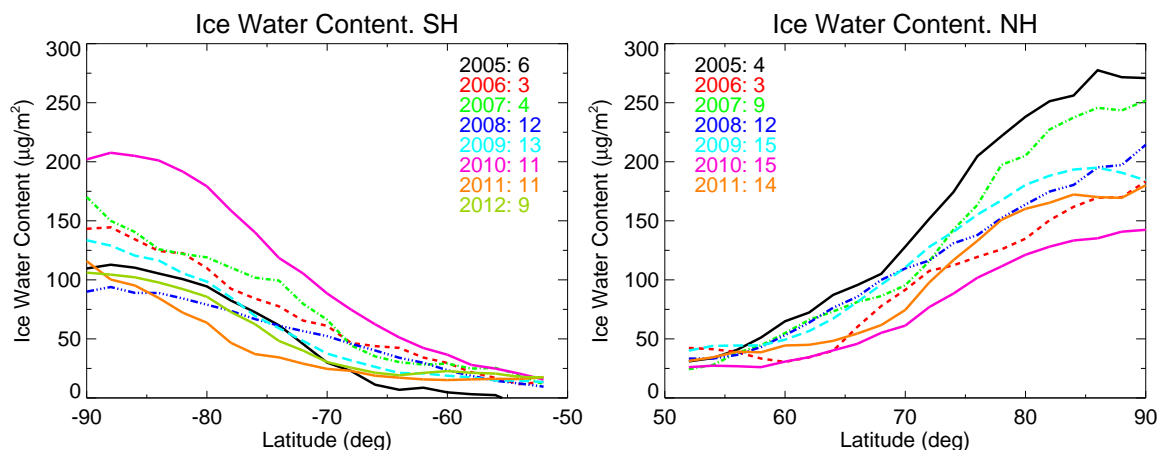


**Figure 8.** Latitudinal distribution of the ice water content of the PMC layers for the SH (left) and the NH (right) seasons for all measurements. The colors indicate the data for different years and the number of days measured per year (see Table 2).

Hervig et al. (2009b, 2013) reported an average value for the mean altitude of the PMC layer of 83.5 km for NH and 84.7 km for SH in SOFIE measurements, and of 83.3 km for the NH from the lidar measurements. The MIPAS mean value obtained here for the NH is very close to both measurements. Also, it is very much in line with SOFIE, locating the maximum of the layer about 1 km higher in the SH than in the NH.

- Russell et al. (2010) carried out a multi-year analysis of the OSIRIS/Odin, SNOE, AIM, and SABER/TIMED data sets in the polar regions north (south) of  $65^\circ\text{N}$  ( $^\circ\text{S}$ ) and found that the mean PMC height is located  $3.5\text{ km} \pm 0.5\text{ km}$  below the mean mesopause height. In the case of SOFIE measurements, however, this difference is significantly smaller, in  $\sim 1\text{ km}$ , for most

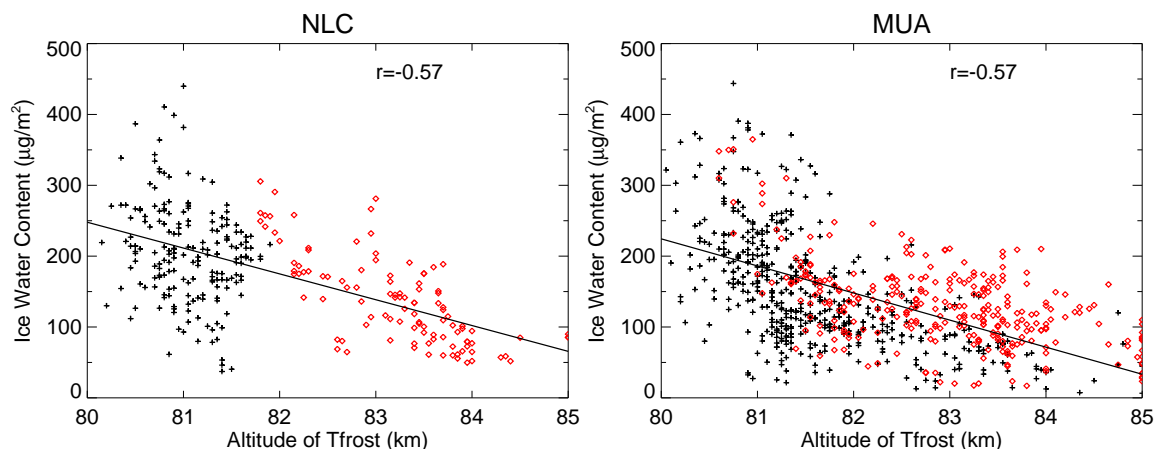


**Figure 9.** Correlation between the ice water content (IWC) and the altitude of the lower branch of the frost point temperature contour (see Fig. 1) for the data taken in the NLC (left panel) and MA+UA (right panel) observation modes in the NH (black pluses) and SH (red diamonds) PMCs seasons (see Table 2).

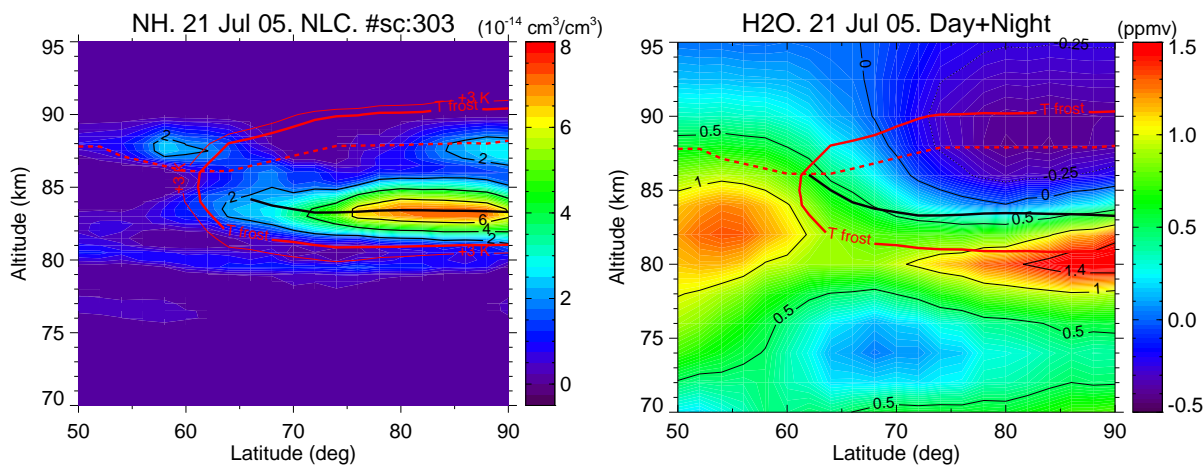


**Figure 10.** Zonal mean of the ice volume density (left) and of the  $\text{H}_2\text{O}$  concentration anomaly (the mean profile has been subtracted) (right) for 21 July 2005. The solid red lines indicate the frost point temperature (thick line) and frost point temperature plus 3 K (thinner line). The red dashed line is the mesopause as measured by MIPAS. The solid black line is an estimated mean altitude of the PMC layer (see Sec. 4).

of the season, except around the middle of the season. We also looked at the difference between the mean PMC height and the mean mesopause height in the MIPAS PMC measurements (see Fig. 7). In general MIPAS observations are more in line with SOFIE observations than with the other instruments. For the case of NLC and MUA MIPAS observation modes in the NH near 70°N, the difference is about 2.5 km, smaller than the mean value of 3.5 km obtained for all instruments and closer to the SOFIE value. It is worth noting that this altitude difference increases towards the North pole, more clearly in the case of the NLC mode (taken around the middle of the season) and reaching about 4 km. In the Southern Hemisphere the difference



between the mesopause and mean ice layer altitudes is even smaller than for NH, with values ranging between 2 and 2.8 km; again in better agreement with SOFIE than with the other instruments.

Figure 8 shows the latitudinal variation of the ice water content of the PMC layer for the SH (left) and the NH (right) seasons for all measurements. The figure shows clearly that PMCs are more abundant in the NH than in the SH, extending to lower latitudes in the NH. The main reason for this is the warmer polar upper mesosphere in the SH than in the NH, about a 10 K difference as measured by MIPAS (García-Comas et al., 2014). As shown in the zonal fields (Figs. 1 and 3), the ice column volume increases toward the poles. The large variability is also clearly visible, which in the case of MIPAS is attributable not only to the yearly changes but also to the daily variation because of the infrequent temporal sampling of MIPAS. The ice column is large for the NLC mode (not shown), in consonance with the zonal mean fields shown in Fig. 3. As mentioned before, this is probably due to the fact that the NLC measurements are taken around the middle of the season (see Table 1). The NH/SH ratio of the ice water content varies with latitude, ranging from about a factor of 2 near 60° to 1.4 near the poles, with a value of 1.7 near 70°, which is in very good agreement with the factor of 65% reported by Hervig et al. (2013) from SOFIE measurements.

## 5 Correlation of ice volume density with the frost point temperature

Figure 9 shows the correlation between the ice water content and the altitude of the lower branch of the frost point temperature contour (see Fig. 1) for the data taken in the different observation modes in the SH and NH PMCs seasons. The correlation is significant and shows that the PMC layers are denser and wider when the frost point temperature occurs at lower altitudes. Furthermore, the ice volume density is also anticorrelated with the mean altitude of the PMC layer (not shown), that is, that the denser PMC layers are located at lower altitudes and the thinner ones at higher altitudes, which is consistent with the behaviours shown in Figs. 7 and 8.

## 6 Correlation of ice volume density with H<sub>2</sub>O concentration

Hervig et al. (2015) suggest that, as opposed to other satellite instruments' like HALOE and MLS water vapour measurements, the vertical resolutions from SOFIE are well suited for the study of correlations between water ice and water vapour. This is also the case for MIPAS. Given the good latitude coverage of MIPAS (covering the whole polar region) and the fact that the instrument is able to measure the ice water content and the water vapour concentration simultaneously, we have looked at the zonal mean and latitudinal/longitudinal distribution of both quantities in the polar summer region. Fig. 10 shows a typical case (21 July 2005) of the zonal mean cross sections of the ice volume density (left) and the H<sub>2</sub>O concentration anomaly (right). Also Fig. 11 shows the latitude/longitude distributions for the H<sub>2</sub>O vmr at 90 km (top) and 80 km (bottom), and for the ice volume density at 83 km (middle). The water vapour concentrations have been derived from MIPAS high resolution spectra in the region around 6.3 μm. We used version v5r\_h2o\_M22 retrievals. The retrieval baseline is an extension to the lower mesosphere of the set-up described by Milz et al. (2005) with the updates described in von Clarmann et al. (2009). The main

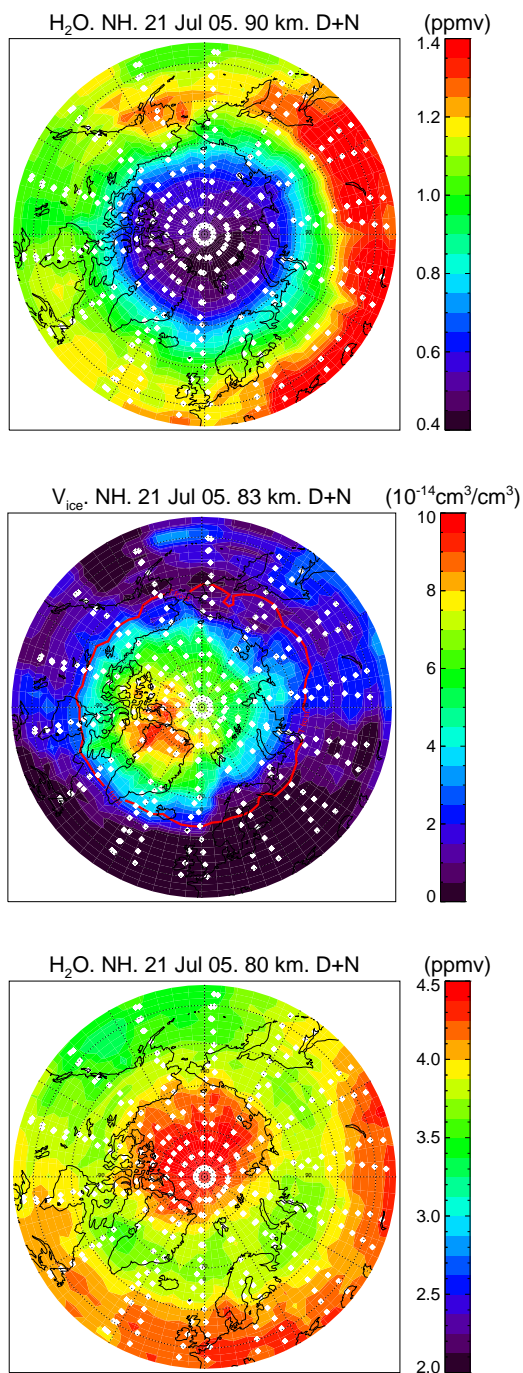


**Figure 11.** Latitude/longitude distribution maps of H<sub>2</sub>O vmr for altitudes of 90 km (top) and 80 km (bottom) (note the different scale) and of ice volume density at 83 km (middle panel) for 21 July 2005 (see Fig. 10).





exhibit a very good latitude/longitude spatial correlation. This topic has been recently studied quantitatively by Hervig et al. (2015) by using SOFIE observation of ice content, water vapour and temperature at latitudes near  $70^\circ$ . They found that, in both hemispheres, the altitude of the peak of the dehydration regions is  $\sim 1.8$  km above the height of peak ice mass density, and the altitude of the peak of the hydration region is  $\sim 0.3$  km above the observed bottom altitude ice layer. Although no general  
5 conclusion can be drawn from the single day of MIPAS data shown here, the location of the hydration region agrees well with SOFIE observations. The dehydration region, however, is found in MIPAS to be significantly higher than in SOFIE (see right panel in Fig. 10).

Hervig et al. (2015) also found that the column abundance of  $\text{H}_2\text{O}$  in the gas phase is roughly equal in the dehydration and hydration layers, but less than that contained in the ice layer. MIPAS data also shows a similar feature, being more  
10 pronounced at latitudes higher than those sounded by SOFIE. The right panel of Fig. 10 shows enhanced values of about 1.5 ppmv in the hydration layer and decreased by 0.5 ppmv in the dehydration region, while the  $Q_{\text{ice}}$  peak is about 6 ppmv. A more comprehensive study, using all MIPAS data, should however be performed to confirm these findings. A further insight provided by MIPAS observations, with respect to SOFIE, is that this layer's structure is more pronounced at latitudes northernmost of  $70^\circ$ .

## 15 7 Diurnal variation of the ice volume density

The diurnal variation of the PMCs is an important factor to be taken into account when comparing the datasets for different PMCs. Several studies have shown that the IWC may have a very large diurnal variation at latitudes close to and equator-wards of  $70^\circ$ , mainly driven by tidal effects in the temperature and in the meridional advection at sub-polar latitudes (Stevens et al., 2010; Gerding et al., 2013). MIPAS measures PMCs at two local times, 10 am and 10 pm, and hence allows us to look at  
20 the diurnal migrating variation (see García-Comas et al., 2016). Fig. 12 shows the diurnal differences (am-pm) of MIPAS ice volume density averaged over all measurements in the SH (left panel) and NH (right panel). The differences are larger in the NH, which are correlated with the larger concentrations in this hemisphere. The am-pm differences in the NH are larger at  $60$ - $80^\circ$ , and reach a maximum value close to  $10^{-14}$   $\text{cm}^3/\text{cm}^3$ . This am enhancement is in line with the predictions of Stevens et al. (2010) but it is not as large as their calculations of a factor of 4.5 in the IWC at  $69^\circ\text{N}$ . At this latitude we find  
25 a maximum daytime enhancement of about 60% in the volume density and 36% in the IWC. Note however that the IWC am-pm differences are also influenced by the slightly negative volume density difference at altitudes above 86 km. The vertically alternating increase at 84 km and decrease at 88 km in the am ice volume density indicates am clouds of lower altitude, also in agreement with Stevens et al. (2010).

The am-pm difference of ice volume density at  $50$ - $60^\circ$  is  $0.25$ - $0.5 \cdot 10^{-14}$   $\text{cm}^3/\text{cm}^3$  at 81-87 km (Fig. 12). That corresponds  
30 to an am/pm ratio lying between 1.5 at 86 km and 7 at 82 km. That indicates a significantly narrower and thinner pm cloud, in agreement with findings at sub-polar latitudes from Stevens et al. (2010) and Gerding et al. (2013), which mainly disappears below 84 km. The corresponding IWC am/pm ratio increases rapidly towards these lower latitudes and varies in the range of 1.5 to 2.8 at  $50$ - $60^\circ$ .



These ice volume density differences are remarkably anti-correlated with the 10 am-10 pm differences in the kinetic temperature measured by MIPAS (bottom panels in Fig. 12) which are a good measure of the temperature perturbations due to the diurnal migrating tide. The negative am-pm difference at 80-85 km at latitudes below 80°N is well anti-correlated to the am-pm ice differences. Also, the temperature differences tend to be positive at higher altitudes northward of 65°, which is well reflected in the ice volume densities. Nevertheless, it is not possible to infer from this correlation alone, and without looking at wind fields, the extent to which these temperature perturbations affect the ice. Influence from other factors, like tidal effects on meridional advection (Gerding et al., 2013, see, e.g.) cannot be ruled out.

The anti-correlation between the diurnal variation of the ice density in the SH (upper left panel in Fig. 12) and that of temperature (lower left panel) is not ubiquitous. In this hemisphere, the negative temperature difference at 50-60°S and 80-84 km is weaker than in the NH. The diurnal positive ice change is correspondingly small but the ice volume density at these latitudes is also very low (less than  $5 \times 10^{-15} \text{ cm}^3/\text{cm}^3$ ). The positive temperature difference above 85 km does anti-correlate with the negative am-pm ice concentration difference at 65-80°S. However, in contrast to the northern hemisphere, the am-pm temperature perturbation at 65-80°S is positive also at 80-85 km but so is the ice variation. This indicates that another factor affects the diurnal ice variation more significantly than temperature at those latitudes, at least below 84 km. Its effect results in vertically alternating positive and negative changes that may lead to larger am-pm cloud altitude differences than in the northern hemisphere. A deeper analysis of this behaviour is beyond the scope of this paper and will be analysed in the future.

## 8 Conclusions

We have analysed the MIPAS IR measurements of PMCs for the summer seasons in the Northern and Southern Hemispheres from 2005 to 2012.

PMCs were measured in the middle IR in emission where, due to the small particle size, the signal is only affected by absorption and not by scattering. It is therefore sensitive to the total ice volume, including the very small ice particles, not generally sounded by the UV-VIS scattering instruments.

The measurements cover only a few days of the PMC season (varying from 3 to 15) but, on the contrary, have a global latitudinal coverage. In this way, MIPAS measurements show, for the first time, global latitudinal coverage (from 50° to the pole) of the total ice volume density.

MIPAS measurements indicate mesospheric ice existing as a continuous layer extending from about ~81 km up to about 88-89 km on average and from the poles to about 55-60° in each hemisphere. These altitudes are in very good agreement with SOFIE measurements, with the lowest altitude being slightly lower (0.5 km) in MIPAS, and the uppermost altitude slightly higher (1-2 km) probably caused by the wider MIPAS field of view. This bottom altitude is also slightly lower than that derived from lidars measurements but the uppermost altitude is significantly higher (4-5 km on average) than that obtained from lidar measurements. This indicates that both MIPAS and SOFIE instruments are sensing the small ice particles at the upper part of the PMC layer which are usually related to polar mesosphere summer echoes. This has also been proved recently by the concurrent observations from the ALOMAR wind (ALWIN) radar and measurements from SOFIE (Hervig et al., 2011).



The PMCs are very variable, both in space and time. On average, MIPAS measurements show that PMCs are confined to latitudes poleward of about  $50\text{--}60^\circ$ , with increasing concentration towards the poles. The water ice content in the PMCs measured by MIPAS at the latitudes of the measurements of SOFIE show, overall, a very good agreement, particularly at the peak of the layer. The water ice content observed by MIPAS is, in general, slightly larger, and also exhibits a larger variability, probably caused by its smaller sensitivity. A distinctive feature, however, is that, in general, MIPAS shows significantly larger values in the region above  $\sim 85$  km, which can be twice those measured by SOFIE. In terms of ice water content, IWC, MIPAS are also generally larger than SOFIE values, principally caused by the larger concentrations above  $\sim 85$  km.

The ice concentration is larger in the Northern Hemisphere than in the Southern Hemisphere. The ratio between the IWC in both hemispheres is also latitude-dependent, varying from a NH/SH ratio of 1.4 close to the poles to a factor of 2.1 around  $60^\circ$ . This also implies that PMCs extend to lower latitudes in the NH.

We have found that the mean altitude of the PMC layer in the NH for the NLC mode of MIPAS observations is located around 83.5–84 km, while in the SH it is about 1 km higher (84.5–85 km). This hemispheric asymmetry is in very good agreement with SOFIE observations (Hervig et al., 2013). For those MIPAS observations taken in the middle and upper atmosphere modes (MA and UA), the mean altitude is higher (in  $\sim 1$  km). This difference is attributed to the coarser sampling and to the broader vertical resolution (particularly in the retrieved temperature) and also to their different temporal sampling since the NLC measurements are usually taken in the middle of the PMC season while MUA are taken earlier and later in the season. A very clear feature in MIPAS observations is that PMCs tend to be at higher altitudes as we move away from the polar region (in both hemispheres), particularly equator-wards of  $70^\circ$ .

MIPAS observations show that the difference between the mean PMC height and the mean mesopause height is about 2.5 km in the NH near  $70^\circ\text{N}$ . This is smaller than the mean value of 3.5 km obtained for several instruments by Russell et al. (2010) and closer to the SOFIE value (Hervig et al., 2013). MIPAS also shows that this altitude difference increases towards the North pole, reaching a value close to 4 km. In the Southern Hemisphere this difference is smaller than for the NH, with values ranging between 2 and 2.8 km; again in better agreement with SOFIE than with the other instruments.

The anti-correlation between the ice water content and the altitude of the lower branch of the frost point temperature contour is significant in MIPAS observations and shows that the PMC layers are denser and wider when the frost point temperature occurs at lower altitudes.

The simultaneous observations of PMCs and water vapour of MIPAS have shown that the PMC layers are surrounded by a hydrated region below and a dehydrated region above. These regions are more pronounced towards the poles, particularly at latitudes northernmost of  $70^\circ\text{N}$ . This global behaviour fits very well with the current picture we have about the PMCs where sequestration of  $\text{H}_2\text{O}$  in the gas phase to form ice leads to a drier atmosphere just above the ice layer, and where the sedimentation of ice and its subsequent sublimation enhances the  $\text{H}_2\text{O}$  gas phase abundance at  $\sim 80$  km. The analysis of a single day of water vapour and PMCs measurements have shown that the location of the hydration region agrees well with SOFIE observations (Hervig et al., 2015). The dehydration region, however, is found to be significantly higher in MIPAS than in SOFIE. Further, as for SOFIE, measured near  $70^\circ$ , MIPAS shows that the column abundance of  $\text{H}_2\text{O}$  in the gas phase is



roughly equal in the dehydration and hydration layers, but less than that contained in the ice layer. MIPAS observations at latitudes north of  $70^\circ$  show that this layering structure is more pronounced.

Finally, MIPAS observations, which are taken at 10 am and 10 pm, also show a diurnal variation in the ice volume density, with larger concentration, and slightly lower altitudes, at am than at pm, in line with the model predictions of Stevens et al. (2010). This diurnal variation is anti-correlated with corresponding differences in temperature in the northern hemisphere, suggesting that it is driven by the temperature migrating diurnal tide, but effects from other factors cannot be ruled out. In the Southern Hemisphere, the lack of anti-correlation with temperature suggests the impact of an additional factor below 84 km.

*Acknowledgements.* We thank Patrick Espy for useful discussions about the temperature of the ice particles. We thank the SOFIE team for providing data, taken from <http://sofie.gats-inc.com/sofie/index.php>. The IAA team was supported by the Spanish MICINN under project ESP2014-54362-P and EC FEDER funds. MGC was financially supported by the MINECO under its 'Ramón y Cajal' subprogram.



## References

- Bailey, S. M., Merkel, A. W., Thomas, G. E., and Carstens, J. N.: Observations of polar mesospheric clouds by the Student Nitric Oxide Explorer, *J. Geophys. Res.*, 110, D13203, doi:10.1029/2004JD005422, 2005.
- Baumgarten, G. and Fiedler, J.: Vertical structure of particle properties and water content in noctilucent clouds, *Geophys. Res. Lett.*, 35, L1081, 2008.
- Berger, U. and Lübken, F.-J.: Trends in mesospheric ice layers in the Northern Hemisphere during 1961–2013, *J. Geophys. Res.*, 120, 2015JD023 355, 2015.
- Berger, U. and von Zahn, U.: Three-dimensional modeling of the trajectories of visible noctilucent cloud particles: An indication of particle nucleation well below the mesopause, *J. Geophys. Res.*, 112, D16204, doi:10.1029/2006JD008106, 2007.
- Berger, U. and Zahn, U. v.: Icy particles in the summer mesopause region: Three-dimensional modeling of their environment and two-dimensional modeling of their transport, *J. Geophys. Res.*, 107, 1366, 2002.
- De Laurentis, M.: Planning of MIPAS new special modes January 2005 Campaign, Tech. rep., ESA Technical Note, ENVI-SPPA-EOPG-TN-05-0002, 2005.
- DeLand, M. T. and Thomas, G. E.: Updated PMC Trends Derived from SBUV Data, *J. Geophys. Res.*, p. 2014JD022253, 2015.
- DeLand, M. T., Shettle, E. P., Thomas, G. E., and Olivero, J. J.: Solar backscattered ultraviolet (SBUV) observations of polar mesospheric clouds (PMCs) over two solar cycles, *J. Geophys. Res.*, 108, 8445, doi:10.1029/2002JD002398, 2003.
- Espy, P. and Jutt, H.: Equilibrium temperature of water-ice aerosols in the high-latitude summer mesosphere, *J. Atmos. Sol.-Terr. Phys.*, 64, 1823–1832, 2002.
- Fiedler, J., Baumgarten, G., and Lübken, F.-J.: NLC observations during one solar cycle above ALOMAR, *J. Atmos. Sol.-Terr. Phys.*, 71, 424–433, 2009.
- Fischer, H., Birk, M., Blom, C., Carli, B., Carlotti, M., von Clarmann, T., Delbouille, L., Dudhia, A., Ehhalt, D., Endemann, M., Flaud, J. M., Gessner, R., Kleinert, A., Koopmann, R., Langen, J., López-Puertas, M., Mosner, P., Nett, H., Oelhaf, H., Perron, G., Remedios, J., Ridolfi, M., Stiller, G., and Zander, R.: MIPAS: an instrument for atmospheric and climate research, *Atmos. Chem. Phys.*, 8, 2151–2188, 2008.
- Funke, B., López-Puertas, M., García-Comas, M., Kaufmann, M., Höpfner, M., and Stiller, G. P.: GRANADA: a Generic Radiative transfer And non-LTE population Algorithm, *J. Quant. Spectrosc. Radiat. Transfer*, doi:10.1016/j.jqsrt.2012.05.001, <http://dx.doi.org/10.1016/j.jqsrt.2012.05.001>, in press, 2012.
- García, R., López-Puertas, M., Funke, B., Kinnison, D. E., Marsh, D. R., and Quian, L.: On the secular trend of CO<sub>x</sub> and CO<sub>2</sub> in the lower thermosphere, *J. Geophys. Res.*, submitted, 2015.
- García-Comas, M., Funke, B., López-Puertas, M., Bermejo-Pantaleón, D., Glatthor, N., Clarmann, T. v., Stiller, G. P., Grabowski, U., Boone, C. D., French, W. J., Leblanc, T., López-González, M. J., and Schwartz, M.: On the Quality of MIPAS Kinetic Temperature in the Middle Atmosphere, *Atmos. Chem. Phys.*, 11, 24 233–24 312, doi:10.5194/acpd-11-24233-2011, 2012.
- García-Comas, M., Funke, B., Gardini, A., López-Puertas, M., Jurado-Navarro, A., von Clarmann, T., Stiller, G. P., Kiefer, M., Boone, C. D., Leblanc, T., Marshall, B. T., Schwartz, M. J., and Sheese, P. E.: MIPAS temperature from the stratosphere to the lower thermosphere: Comparison of vM21 with ACE-FTS, MLS, OSIRIS, SABER, SOFIE and lidar measurements, *Atmospheric Measurement Techniques*, 7, 3633–3651, 2014.



- García-Comas, M., González-Galindo, F., Funke, B., Gardini, A., Jurado-Navarro, A. A., López-Puertas, M., and Ward, W. E.: MIPAS observations of longitudinal oscillations in the mesosphere and the lower thermosphere: Part 1. Climatology of odd-parity daily frequency modes, *Atmos. Chem. Phys.*, in review, 2016.
- García-Comas, M., Funke, B., López-Puertas, M., Lossow, S., Gabriele, S., von Clarmann, T., Glatthor, N., and Grabowski, U.: Measurements of Water Vapor Distribution in the Middle Atmosphere by MIPAS, in: *Advances in Atmospheric Science and Applications*, edited by ESA, vol. ATMOS 2012 Abstract Book, pp. 88–89, ESA, 2012.
- Gerding, M., Kopp, M., Hoffmann, P., Höffner, J., and Lübken, F.-J.: Diurnal variations of midlatitude NLC parameters observed by daylight-capable lidar and their relation to ambient parameters, *Geophys. Res. Lett.*, 40, 6390–6394, doi:10.1002/2013GL057955, 2013.
- Grossmann, K. U., Gusev, O., Assou, M. A., and Witt, G.: Spectral emission measurements of polar mesospheric clouds by CRISTA–2, *J. Atmos. Solar–Terr. Phys.*, 68, 1781–1790, doi:10.1016/j.jastp.2006.01.014, 2006.
- Gumbel, J. and Witt, G.: In situ measurements of the vertical structure of a noctilucent cloud, *Geophys. Res. Lett.*, 25, 493–496, 1998.
- Hervig, M. and Gordley, L. L.: Temperature, shape, and phase of mesospheric ice from Solar Occultation for Ice Experiment observations, *J. Geophys. Res.*, 115, D15 208, 2010.
- Hervig, M., Thompson, R. E., McHugh, M., Gordley, L. L., Russell III, J. M., and Summers, M. E.: First confirmation that water ice is the primary component of polar mesospheric clouds, *Geophys. Res. Lett.*, 28, 971–974, 2001.
- Hervig, M., McHugh, M., and Summers, M. E.: Water vapor enhancement in the polar summer mesosphere and its relationship to polar mesospheric clouds, *Geophys. Res. Lett.*, 30, 2041, doi:10.1029/2003GL018089, 2003.
- Hervig, M. E. and Stevens, M. H.: Interpreting the 35 year SBUV PMC record with SOFIE observations, *J. Geophys. Res.*, 119, 2014JD021 923, 2014.
- Hervig, M. E., Gordley, L. L., Russell, III, J. M., and Bailey, S. M.: SOFIE PMC observations during the northern summer of 2007, *J. Atmos. Sol.-Terr. Phys.*, 71, 331–339, 2009a.
- Hervig, M. E., Gordley, L. L., Stevens, M. H., Russell, III, J. M., Bailey, S. M., and Baumgarten, G.: Interpretation of SOFIE PMC measurements: Cloud identification and derivation of mass density, particle shape, and particle size, *J. Atmos. Sol.-Terr. Phys.*, 71, 316–330, 2009b.
- Hervig, M. E., Stevens, M. H., Gordley, L. L., Deaver, L. E., Russell, III, J. M., and Bailey, S. M.: Relationships between polar mesospheric clouds, temperature, and water vapor from Solar Occultation for Ice Experiment (SOFIE) observations, *J. Geophys. Res.*, 114, D20 203, 2009c.
- Hervig, M. E., Rapp, M., Latteck, R., and Gordley, L. L.: Observations of mesospheric ice particles from the ALWIN radar and SOFIE, *J. Atmos. Sol.-Terr. Phys.*, 73, 2176–2183, 2011.
- Hervig, M. E., Siskind, D. E., Stevens, M. H., and Deaver, L. E.: *J. Atmos. Sol.-Terr. Phys.*, *J. Atmos. Sol.-Terr. Phys.*, 104, 285–298, 2013.
- Hervig, M. E., Siskind, D. E., Bailey, S. M., and Russell, III, J. M.: The influence of PMCs on water vapor and drivers behind PMC variability from SOFIE observations, *J. Atmos. Sol.-Terr. Phys.*, 132 IS -, 124–134, 2015.
- López-Puertas, M., García-Comas, M., Funke, B., Bermejo-Pantaleón, D., Höpfner, M., Grabowski, U., Stiller, G. P., von Clarmann, T., and von Savigny, C.: Measurements of polar mesospheric clouds in infrared emission by MIPAS/ENVISAT, *J. Geophys. Res.*, 114, D00I07, doi:10.1029/2009JD012548, 2009.
- Lübken, F.-J.: Thermal structure of the arctic summer mesosphere, *J. Geophys. Res.*, 104, 9135–9150, doi:10.1029/1999JD900076, 1999.



- Määttänen, A., Perot, K., Montmessin, F., and Hauchecorne, A.: Mesospheric Clouds on Mars and on Earth, in: Comparative climatology of terrestrial planets, edited by J. M. S., Simo-Miller, A. A., Harder, J. W., Bullock, M. A., and Dotson, R., pp. 393–413, University of Arizona Press, Tucson, Arizona, 2013.
- Milz, M., von Clarmann, T., Fischer, H., Glatthor, N., Grabowski, U., Höpfner, M., Kellmann, S., Kiefer, M., Linden, A., Mengistu  
5 Tsidu, G., Steck, T., Stiller, G. P., Funke, B., López-Puertas, M., and Koukoulis, M. E.: Water Vapor Distributions Measured with the Michelson Interferometer for Passive Atmospheric Sounding on board Envisat (MIPAS/Envisat), *J. Geophys. Res.*, 110, D24307, doi:10.1029/2005JD005973, 2005.
- Nedoluha, G. E., Gomez, R. M., Hicks, B. C., Wrotny, J. E., Boone, C., and Lambert, A.: Water vapor measurements in the mesosphere from Mauna Loa over solar cycle 23, *J. Geophys. Res.*, 114, D23 303, 2009.
- 10 Oelhaf, H.: MIPAS Mission Plan, ESA Technical Note ENVI-SPPA-EOPG-TN-07-0073, 2008.
- O’Neil, R. R., Richards, E., Humphrey, C. H., and Stair, A. T.: Polar mesospheric clouds: Infrared measurements from the Midcourse Space Experiment, *J. Geophys. Res.*, 113, A07 303, 2008.
- Pérot, K., Hauchecorne, A., Montmessin, F., Bertaux, J.-L., Blanot, L., Dalaudier, F., Fussen, D., and Kyrölä, E.: First climatology of polar mesospheric clouds from GOMOS/ENVISAT stellar occultation instrument, *Atmospheric Chemistry and Physics*, 10, 2723–2735, 2010.
- 15 Petelina, S., Llewellyn, E. J., Degenstein, D. A., and Lloyd, N. D.: Odin/OSIRIS limb observations of polar mesospheric clouds in 2001–2003, *J. Atmos. Solar-Terr. Phys.*, 68, 42–55, doi:10.1016/j.jastp.2005.08.004, 2006.
- Petelina, S. V. and Zasetsky, A. Y.: Temperature of mesospheric ice retrieved from the O-H stretch band, *Geophys. Res. Lett.*, 36, L15 804, 2009.
- Rapp, M. and Lübken, F.-J.: Polar mesosphere summer echoes (PMSE): review of observations and current understanding, *Atmos. Chem. Phys.*, 4, 2601–2633, 2004.
- 20 Rapp, M. and Thomas, G.: Modeling the microphysics of mesospheric ice particles: Assessment of current capabilities and basic sensitivities, *J. Atmos. Sol.-Terr. Phys.*, 68, 715–744, 2006.
- Roble, R. G. and Dickinson, R. E.: How will changes in carbon dioxide and methane modify the mean structure of the mesosphere and thermosphere?, *Geophys. Res. Lett.*, 16, 1441–1444, 1989.
- 25 Rusch, D. W., Thomas, G. E., and Jensen, E. J.: Particle Size Distributions in Polar Mesospheric Clouds Derived From Solar Mesosphere Explorer Measurements, *J. Geophys. Res.*, 96, 12,933–12,939, 1991.
- Russell, III, J. M., Rong, P., Bailey, S. M., Hervig, M. E., and Petelina, S. V.: Relationship between the summer mesopause and polar mesospheric cloud heights, *J. Geophys. Res.*, 115, D16 209, 2010.
- Russell, III, J. M., Rong, P., Hervig, M. E., Siskind, D. E., Stevens, M. H., Bailey, S. M., and Gumbel, J.: Analysis of northern midlatitude  
30 noctilucent cloud occurrences using satellite data and modeling, *J. Geophys. Res.*, 119, 3238–3250, 2014.
- Russell III, J. M., Bailey, S. M., Gordley, L. L., Rusch, D. W., Horányi, M., Hervig, M. E., Thomas, G. E., Randall, C. E., Siskind, D. E., Stevens, M. H., Summers, M. E., Taylor, M. J., Englert, C. R., Espy, P. J., McClintock, W. E., and Merkel, A. W.: The Aeronomy of Ice in the Mesosphere (AIM) mission: Overview and early science results, *J. Atmos. Sol.-Terr. Phys.*, 71, 289–299, 2009.
- Stevens, M. H., Siskind, D. E., Eckermann, S. D., Coy, L., McCormack, J. P., Englert, C. R., Hoppel, K. W., Nielsen, K., Kochenash, A. J.,  
35 Hervig, M. E., Randall, C. E., Lumpe, J., Bailey, S. M., Rapp, M., and Hoffmann, P.: Tidally induced variations of polar mesospheric cloud altitudes and ice water content using a data assimilation system, *J. Geophys. Res.*, 115, 2010.



- Stiller, G. P., von Clarmann, T., Funke, B., Glatthor, N., Hase, F., Höpfner, M., and Linden, A.: Sensitivity of trace gas abundances retrievals from infrared limb emission spectra to simplifying approximations in radiative transfer modelling, *J. Quant. Spectrosc. Radiat. Transfer*, 72, 249–280, doi:10.1016/S0022-4073(01)00123-6, 2002.
- Stiller, G. P., Kiefer, M., Eckert, E., von Clarmann, T., Kellmann, S., García-Comas, M., Funke, B., Leblanc, T., Fetzer, E., Froidevaux, L., Gomez, M., Hall, E., Hurst, D., Jordan, A., Kämpfer, N., Lambert, A., McDermid, I. S., McGee, T., Miloshevich, L., Nedoluha, G., Read, W., Schneider, M., Schwartz, M., Straub, C., Toon, G., Twigg, L. W., Walker, K., and Whiteman, D. N.: Validation of MIPAS IMK/IAA temperature, water vapor, and ozone profiles with MOHAVE-2009 campaign measurements, *Atmos. Meas. Tech.*, 5, 289–320, doi:10.5194/amt-5-289-2012, www.atmos-meas-tech.net/5/289/2012/, 2012.
- Thomas, G. E.: Are Noctilucent Clouds Harbingers of Global Change in the Middle Atmosphere?, *Adv. Space Res.*, 32, 1737–1746, doi:10.1016/S0273-1177(03)00674-4, 2003.
- Thomas, G. E., Olivero, J. J., Jensen, E. J., Schroeder, W., and Toon, O. B.: Relation between increasing methane and the presence of ice clouds at the mesopause, *Nature*, 338, 490, 1989.
- Thomas, G. E., Thurairajah, B., Hervig, M. E., von Savigny, C., and Snow, M.: Solar-induced 27-day variations of mesospheric temperature and water vapor from the AIM SOFIE experiment: Drivers of polar mesospheric cloud variability, *J. Atmos. Sol.-Terr. Phys.*, 134 IS -, 56–68, 2015.
- Tikhonov, A.: On the solution of incorrectly stated problems and method of regularization, *Dokl. Akad. Nauk. SSSR*, 151, 501–504, 1963.
- Toon, O. B., Tolbert, M. A., Koehler, B. G., Middlebrook, A. M., and Jordan, J.: Infrared optical constants of H<sub>2</sub>O ice, amorphous nitric acid solutions, and nitric acid trihydrates, *J. Geophys. Res.*, 99, 25,631–25,654, 1994.
- von Clarmann, T., Glatthor, N., Grabowski, U., Höpfner, M., Kellmann, S., Kiefer, M., Linden, A., Mengistu Tsidu, G., Milz, M., Steck, T., Stiller, G. P., Wang, D. Y., Fischer, H., Funke, B., Gil-López, S., and López-Puertas, M.: Retrieval of temperature and tangent altitude pointing from limb emission spectra recorded from space by the Michelson Interferometer for Passive Atmospheric Sounding (MIPAS), *J. Geophys. Res.*, 108, 4736, doi:10.1029/2003JD003602, 2003.
- von Clarmann, T., Höpfner, M., Kellmann, S., Linden, A., Chauhan, S., Grabowski, U., Funke, B., Glatthor, N., Kiefer, M., Schieferdecker, T., and Stiller, G. P.: Retrieval of temperature H<sub>2</sub>O, O<sub>3</sub>, HNO<sub>3</sub>, CH<sub>4</sub>, N<sub>2</sub>O and ClONO<sub>2</sub> from MIPAS reduced resolution nominal mode limb emission measurements, *Atmos. Meas. Tech.*, 2, 159–175, 2009.
- von Cossart, G., Fiedler, J., and von Zahn, U.: Size distributions of NLC particles as determined from 3-color observations of NLC by ground-based lidar, *Geophys. Res. Lett.*, 26, 1513–1516, 1999.
- von Savigny, C. and Burrows, J. P.: Latitudinal variations of NLC particle radii derived from northern hemisphere SCIAMACHY/Envisat limb measurements, *Adv. Space Res.*, 40, 765–771, doi:10.1016/j.asr.2006.12.032, 2007.
- von Savigny, C., Petelina, S. V., Karlsson, B., Llewellyn, E. J., Degenstein, D. A., Lloyd, N. D., and Burrows, J. P.: Vertical variation of NLC particle sizes retrieved from Odin/OSIRIS limb scattering observations, *Geophys. Res. Lett.*, 32, L07806, doi:10.1029/2004GL021982, 2005.
- von Savigny, C., Robert, C., Bovensmann, H., Burrows, J. P., and Schwartz, M.: Satellite observations of the quasi 5–day wave in noctilucent clouds and mesopause temperatures, *Geophys. Res. Lett.*, 34, L24808, doi:10.1029/2007GL030987, 2007.
- von Zahn, U.: Are noctilucent clouds truly a “miners canary” of global change?, *EOS Trans. AGU*, 84, 261, 2003.
- Yue, J., Russell, III, J. M., Jian, Y., Rezac, L., Garcia, R. R., López-Puertas, M., and Mlynczak, M. G.: Increasing carbon dioxide concentration in the upper atmosphere observed by SABER, *Geophys. Res. Lett.*, 42, 1–6, 2015.